Dynamics of ion shielding in an anisotropic electron plasma

Gang Wang* and Michael Blaskiewicz
Brookhaven National Laboratory, Upton, New York 11973, USA
(Received 3 April 2008; revised manuscript received 12 June 2008; published 22 August 2008)

We show that, for a test ion moving in a collisionless single-species electron plasma, exact analytical solutions can be obtained for certain anisotropic velocity distributions of the electron plasma. By comparing the analytical formula with the numerical results calculated for the more realistic Maxwellian plasma, we demonstrate that plasmas with three different velocity distributions behave similarly for ions moving with velocity smaller than the velocity spread of the electrons. Furthermore, we show that the response of the electron density to a rest ion decays exponentially with distance, provided the anisotropic velocity distribution exhibits elliptical symmetry.

DOI: 10.1103/PhysRevE.78.026413 PACS number(s): 52.27.Aj

I. INTRODUCTION

The new concept of beam cooling, viz., coherent electron cooling (CEC), has greatly accelerated interest in the shielding effects of anisotropic plasma for moving ions. As an effective way of significantly increasing the luminosity of modern accelerators, the idea of CEC was proposed by Derbenev in 1980 [1] and a novel scheme with full evaluation was recently developed by Litvinenko and Derbenev [2]. The first step of CEC, modulating the electron beam, is realized by the ion shielding, i.e., the electron-density response to moving ions. A few facts make the well-established asymptotic theory for slow-moving ions inapplicable to the process [3–8]. First, since the proposed interaction time of the modulation is only about $\frac{1}{4}-\frac{1}{2}$ of the plasma oscillation, the transient effects could not be sufficiently Landau damped and hence the system would not yet reach its equilibrium. Second, the electron beam has very different longitudinal and transversal thermal temperatures that make it an anisotropic system. Lastly, as the thermal velocity of the ions and electrons is comparable, the solution should also apply to ions moving with velocity comparable to the thermal velocity of the electrons. Accordingly, we need a more generally applicable dynamical description of ion shielding in an anisotropic nonequilibrium plasma to understand the physics of the modulation and estimate its efficiency. By solving the linearized Vlasov-Poisson equations in the time domain, we found exact analytic solutions for Lorentzian plasmas. For a rest ion, the analytic solutions are reduced to the well-known Debye screening formula at $t\rightarrow\infty$. To assess the validity of the analytic formula, we explore the thermal assumption by comparing it with the numerical solution for the Maxwellian plasma.

The content of this paper is organized as follows. In Sec. II, we show that the linearized Vlasov-Poisson equation system is equivalent to an integral equation in the time domain. In Sec. III, the analytic solutions are derived for two different types of thermal distribution, the second power and the third power of the Lorentzian distribution. Section IV presents the numerical solution for the Maxwellian plasma and compares it with the analytic solutions. We demonstrate that the third power of the Lorentzian distribution agrees better with the numerical result than the second power and qualitatively gives the correct dependence of the damping rate and plasma frequency on wavelength, especially in the long-wavelength region. We also show that the density response of an anisotropic plasma to a rest ion decays exponentially with distance, provided the velocity distribution of the plasma retains its elliptical symmetry. In Sec. V, we compare the dynamical solution with the asymptotic solution in the wave-vector domain and the steady-state solution in the space domain [6–8]. It is shown that the dynamical solution agrees very well with the steady-state solutions at $\omega_p t \gg 2\pi$ for the Maxwellian plasma. Section VI contains our summary.

II. VLASOV-POISSON EQUATIONS

In the linear region, the density variation of the electron beam is the superposition of the responses induced by each individual ion. Neglecting the boundary effects and taking into account the short interaction time, we can simplify the modulation process to the shielding of a single ion moving in an infinite single-species electron plasma with constant velocity. If the variation in plasma density is small compared to its equilibrium background, the higher-order terms can be ignored and the system can be described with the linearized Vlasov equation

$$\frac{\partial}{\partial t}f_1(\vec{x},\vec{v},t)+\vec{v}\cdot\frac{\partial}{\partial\vec{x}}f_1(\vec{x},\vec{v},t)-\frac{e\vec{E}}{m_e}\cdot\frac{\partial}{\partial\vec{v}}f_0(\vec{v})=0, \quad (1)$$

where $f_1(\vec{x},\vec{v},t)$ is the perturbation of electron density in the phase space and $f_0(\vec{v})$ is the velocity distribution of the electron background which has uniform spatial distribution with electron density n_0. Assuming that the thermal velocity of the electrons that is small compared with the speed of light, then the magnetic field may also be ignored, thereby reducing the Maxwell equations to the Poisson equation,

$$\vec{\nabla}\cdot\vec{E}(\vec{x},t)=\frac{\rho(\vec{x},t)}{\epsilon_0}. \quad (2)$$

*Also at Physics Department, State University of New York at Stony Brook, Stony Brook, NY. gawang@bnl.gov

Considering that the external electric field is caused by an ion, the charge density in the rest frame of the ion is given by

$$\rho(\vec{x},t) = Z_i e\,\delta(\vec{x}) - e\tilde{n}_1(\vec{x},t), \tag{3}$$

where $\tilde{n}_1(\vec{x},t)=\int f_1(\vec{x},\vec{v},t)d^3v$. Equations (1)–(3) form a self-consistent description of the electron plasma driven by a moving ion, which then is Fourier transformed into the wave-vector space as

$$\frac{\partial}{\partial t}f_1(\vec{k},\vec{v},t) + i\vec{k}\cdot\vec{v}f_1(\vec{k},\vec{v},t) + i\frac{e\Phi(\vec{k},t)}{m_e}\vec{k}\cdot\frac{\partial}{\partial\vec{v}}f_0(\vec{v}) = 0, \tag{4}$$

where

$$\Phi(\vec{k},t) = \frac{e}{\epsilon_0 k^2}[Z_i - \tilde{n}_1(\vec{k},t)] \tag{5}$$

is the Fourier component of the electric potential and the system is transformed into the ion rest frame. Multipling both sides of Eq. (4) by $e^{i\vec{k}\cdot\vec{v}t}$ gives

$$\frac{\partial}{\partial t}[e^{i\vec{k}\cdot\vec{v}t}f_1(\vec{k},\vec{v},t)] = -i\frac{e}{m_e}\Phi(\vec{k},t)e^{i\vec{k}\cdot\vec{v}t}\left(\vec{k}\cdot\frac{\partial}{\partial\vec{v}}f_0(\vec{v})\right). \tag{6}$$

Considering the initial condition $f_1(\vec{k},0)=0$, the integration of Eq. (6) generates

$$f_1(\vec{k},\vec{v},t) = -i\frac{e}{m_e}\int_0^t \Phi(\vec{k},t_1)e^{i\vec{k}\cdot\vec{v}(t_1-t)}\vec{k}\cdot\frac{\partial}{\partial\vec{v}}f_0(\vec{v})dt_1. \tag{7}$$

Integrating Eq. (7) over the three-dimensional electron velocities, and noting the relation

$$i\int\frac{\vec{k}}{k^2}\cdot\frac{\partial}{\partial\vec{v}}f_0(\vec{v})e^{i\vec{k}\cdot\vec{v}\tau}d^3v = \int f_0(\vec{v})e^{i\vec{k}\cdot\vec{v}\tau}\tau\,d^3v,$$

we finally obtain an integral equation in the wave-vector space [9,10].

$$\tilde{n}_1(\vec{k},t) = \omega_p^2\int_0^t[\tilde{n}_1(\vec{k},t_1) - Z_i](t_1-t)g(\vec{k}(t-t_1))dt_1, \tag{8}$$

where

$$g(\vec{u}) \equiv \frac{1}{n_0}\int f_0(\vec{v})e^{-i\vec{u}\cdot\vec{v}}d^3v \tag{9}$$

and $\omega_p=\sqrt{n_0e^2/m_e\epsilon_0}$. To progress further analytically, the electrons' velocity distribution must be specifically chosen such that Eq. (8) is solvable.

III. ANALYTICAL SOLUTIONS FOR A LORENTZIAN PLASMA

A. The second power of the Lorentzian distribution

We consider an electron plasma having the following velocity distribution:

$$f_0(\vec{v}) = \frac{n_0}{\pi^2\beta_x\beta_y\beta_z}\left(1 + \frac{(v_x+v_{0x})^2}{\beta_x^2} + \frac{(v_y+v_{0y})^2}{\beta_y^2} + \frac{(v_z+v_{0z})^2}{\beta_z^2}\right)^{-2}, \tag{10}$$

where β_x, β_y, and β_z are the parameters describing the plasma's three-dimensional temperatures and $\vec{v}_0$ is the ion's velocity with respect to the average velocity of the electron background. The distribution of Eq. (10) is essentially the second power of the Lorentzian distribution and it gives

$$g(\vec{u}) = \exp[i\vec{u}\cdot\vec{v}_0 - R(\vec{u})], \tag{11}$$

where $R(\vec{u}) \equiv \sqrt{(u_x\beta_x)^2+(u_y\beta_y)^2+(u_z\beta_z)^2}$. Inserting Eq. (11) into Eq. (8) and multiplying both sides of the equation by a common factor $e^{-\lambda(\vec{k})t}$ yields

$$\tilde{H}_1(\vec{k},t) = \omega_p^2\int_0^t[\tilde{H}_1(\vec{k},t_1) - Z_ie^{-\lambda(\vec{k})t_1}](t_1-t)dt_1, \tag{12}$$

where

$$\lambda(\vec{k}) = i\vec{k}\cdot\vec{v}_0 - \sqrt{(k_x\beta_x)^2+(k_y\beta_y)^2+(k_z\beta_z)^2} \tag{13}$$

and

$$\tilde{H}_1(\vec{k},t) = \tilde{n}_1(\vec{k},t)e^{-\lambda(\vec{k})t}. \tag{14}$$

Taking the second time derivative for both sides of Eq. (12) gives the following inhomogeneous second-order ordinary differential equation (ODE) with constant coefficients:

$$\frac{d^2}{dt^2}\tilde{H}_1(\vec{k},t) + \omega_p^2\tilde{H}_1(\vec{k},t) = \omega_p^2Z_ie^{-\lambda(\vec{k})t}. \tag{15}$$

The solution of Eq. (15) comprises homogeneous oscillation parts and an exponential part from the inhomogeneous term. After considering the zero initial conditions, $\tilde{n}_1(\vec{k},0)=0$ and $\dot{\tilde{n}}_1(\vec{k},t)=0$, the solution for $\tilde{n}_1(\vec{k},t)$ can be obtained as

$$\tilde{n}_1(\vec{k},t) = \frac{\omega_p^2}{\omega_p^2+\lambda(\vec{k})^2}\left[1 - e^{\lambda(\vec{k})t}\left(\cos(\omega_pt) - \frac{\lambda(\vec{k})}{\omega_p}\sin(\omega_pt)\right)\right]. \tag{16}$$

The second term in the large parentheses shows the transient plasma oscillation induced by the ion's presence. The oscillation is Landau damped after a few plasma oscillations, and only those components with a very long wavelength remain oscillating as shown in Fig. 1. The first derivative of Eq. (16) reads

$$\dot{\tilde{n}}_1(\vec{k},t) = Z_i\omega_p\sin(\omega_pt)e^{\lambda(\vec{k})t}. \tag{17}$$

The Fourier inversion of Eq. (17) generates the time derivative of the electron-density variation,

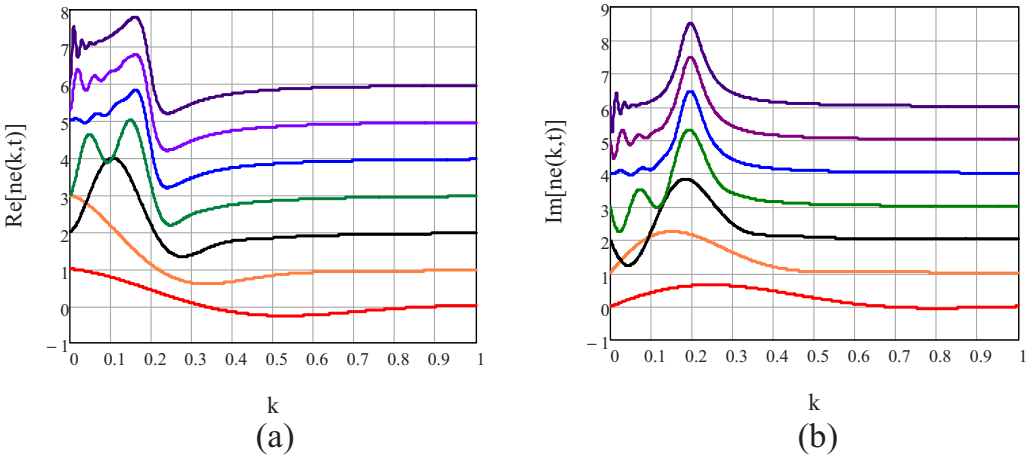

FIG. 1. (Color online) Mountain range plot for the electron response $\tilde{n}_1(\vec{k},t)$ as a function of the wave number and time. The horizontal axis is the normalized wave number as defined in Eq. (25). The graph depicts the ion's velocity and the wave vector $\vec{k}$ along the z direction, and $|\bar{v}_{0z}|=5\beta_z$. Starting from the bottom, the snapshos are taken at $\psi/\pi=0.5,1,2,4,7.5,10.25,20$. Each curve is shifted vertically by one grid with respect to its prior curve to show the time dependence.

$$\tilde{n}_1(\vec{x},t)=\frac{Z_i(\beta_x\beta_y\beta_z)^{-1}\omega_p t\sin(\omega_p t)}{\pi^2\left(t^2+\dfrac{(x+v_{0x}t)^2}{\beta_x^2}+\dfrac{(y+v_{0y}t)^2}{\beta_y^2}+\dfrac{(z+v_{0z}t)^2}{\beta_z^2}\right)^2}. \tag{18}$$

Taking into account the initial conditions, the electron density response is derived as the following one-dimentional integration:

$$\tilde{n}_1(\vec{\bar{x}},\psi)=\frac{Z_i}{\pi^2 a_x a_y a_z}\int_0^{\psi}\psi_1\sin(\psi_1)[\psi_1^2+(\bar{x}+\bar{v}_{0x}\psi_1)^2+(\bar{y}+\bar{v}_{0y}\psi_1)^2+(\bar{z}+\bar{v}_{0z}\psi_1)^2]^{-2}d\psi_1, \tag{19}$$

wherein the normalized variables are defined as $\psi\equiv\omega_p t$, $a_i\equiv\beta_i/\omega_p$, $\bar{x}_i\equiv x_i/a_i$, $\bar{v}_{0i}\equiv v_{0i}/\beta_i$, and $i=x,y,z$. Equation (19) essentially is the sum of a few sinusoidal integrals and no further significant simplification can be made analytically. Figure 2 plots the results of numerical integration for Eq. (19). The snapshots at $\psi=\pi$ are shown for a rest ion and a moving ion with $v_{0z}=10\beta_z$. Actually, in the case of $\vec{v}_0=0$ and $t\to\infty$, Eq. (19) reduces to the following equilibrium solution:

$$\tilde{n}_1(\vec{x})=\frac{Z_i}{\pi^2 a_x a_y a_z}\int_0^{\infty}\frac{\psi\sin\psi d\psi}{(\psi^2+\bar{r}^2)^2}=\frac{Z_i}{4\pi a_x a_y a_z}\frac{1}{\bar{r}}e^{-\bar{r}}, \tag{20}$$

where $\bar{r}=\sqrt{\bar{x}^2+\bar{y}^2+\bar{z}^2}$. Equation (20) predicts that the electron density modulation decays exponentially with distance. When the three temperatures in each direction are the same, Eq. (18) reproduces the well-known Debye screening formula. Figure 3 shows the time evolution of the electron response to an ion moving with velocity $\bar{v}_0=5$. Since Landau damping is efficient for the short-wavelength component, the local density around the ion stops varying after $\frac{1}{2}$ of the plasma oscillation.

Figure 2(b) demonstrates the tendency of the charge distribution to concentrate into a smaller cone as the ion veloc-

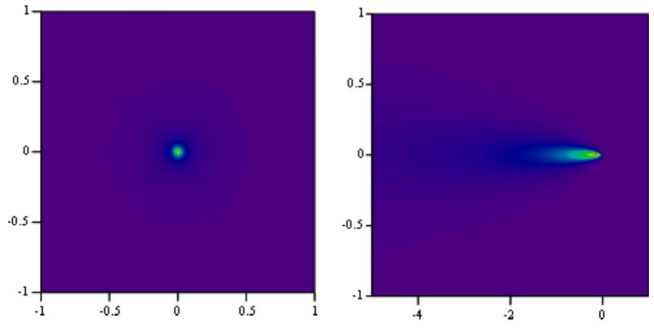

FIG. 2. (Color online) Response of the second-power Lorentzian plasma to an ion. The horizontal and vertical axes are, respectively, the normalized spatial coordinates x and y in units of their Debye radiis a_x and a_y. The left graph is for a rest ion and the right for an ion with velocity $v_{0z}=10\beta_z$. The snapshot is taken at $\psi=\pi$.

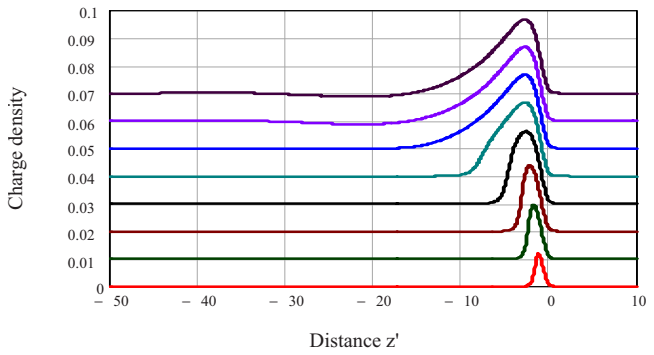

FIG. 3. (Color online) Mountain range plot for the electron response $\tilde{n}_1(\vec{\bar{x}},\psi)$ as a function of the longitudinal location and time. The graph represents the transverse location $\bar{x}=\bar{y}=0.3$. Starting from the bottom, the snapshots are taken at $\psi/\pi=0.1,0.15,0.2,0.3,0.5,1,2.5,10$. Each curve is shifted vertically by one grid with respect to its prior curve to show the time dependence.

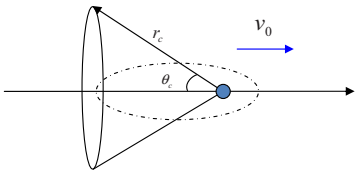

FIG. 4. (Color online) Integration volume V_{cone} of Eq. (21). r_c and θ_c are the integration radius and angle cutoff, respectively. The ion is moving with velocity v_0 and the induced charge within the backward cone is to be calculated.

ity increases. This effect is verified by integrating Eq. (19) over a certain solid angle and radius, as shown in Fig. 4. The integration can be carried out analytically and expressed in the following form:

$$\tilde{Q}(\theta_c,\bar{r}_c,\psi) = \int\int\int_{V_{\text{cone}}} \tilde{n}_1(\vec{x},\psi)dV$$
$$= \frac{Z_i e}{\pi a_x a_y a_z}\int_0^{\psi} \psi_1 \sin(\psi_1)[I(0,\bar{r}_c,\psi_1) - I(\theta_c,\bar{r}_c,\psi_1)]d\psi_1, \quad (21)$$

where

$$I(\theta_c,\bar{r}_c,\psi) = \frac{\text{Im}\left[\bar{r}_0 \ln\left(1-\frac{\bar{r}_c}{\bar{r}_0}\right)\right]}{\psi^2\bar{v}_0\sqrt{1+\bar{v}_0^2\sin^2\theta_c}}$$

and

$$\bar{r}_0 = \bar{v}_0\psi\cos\theta_c + i\psi\sqrt{1+\bar{v}_0^2\sin^2\theta_c}$$

Figure 5 shows the numerical integration results of Eq. (21). In Fig. 5(a), we plot as a function of time the total electron charge induced by an ion moving with velocity $\bar{v}_0=1$ inside a sphere with radius $\bar{r}_c=2$. Reaching its maximum after $\frac{1}{4}-\frac{1}{2}$ plasma oscillations, the total induced charge around the ion remains almost constant. The effects of velocity on the charge distribution are shown in Fig. 5(b). For example, as the velocity increases to $\bar{v}_0=5$, 80% of the total induced charge is concentrated into the backward cone with $\theta_c=\pi/5$.

We note that the distribution described in Eq. (10) has some drawbacks. Although the plasma oscillation and Landau damping are described in Eq. (16), their wavelength dependence is quite different from that of a Maxwellian plasma. Actually the distribution of Eq. (10) does not even define the rms spread of the velocity distribution. To obtain analytic results that are more realistic and closer to the Maxwellian plasma, we consider the third power of the Lorentzian distribution.

B. The third power of the Lorentzian distribution

The normalized velocity distribution of the third-power Lorentzian distribution reads

$$f_0(\vec{v}) = \frac{4n_0}{\pi^2\beta_x\beta_y\beta_z}\left(1+\frac{(v_x+v_{0x})^2}{\beta_x^2}+\frac{(v_y+v_{0y})^2}{\beta_y^2}+\frac{(v_z+v_{0z})^2}{\beta_z^2}\right)^{-3}. \quad (22)$$

Inserting Eq. (25) into Eq. (9) yields

$$g(\vec{u}) = [1+R(\vec{u})]e^{i\vec{u}\cdot\vec{v}_0-R(\vec{u})}, \quad (23)$$

where $R(\vec{u})$ is the same as defined in Eq. (11). Following similar steps as in the previous section, we obtain the following third-order ODE with constant coefficients

$$\tilde{H}_1''' + \tilde{H}_1' + 2\bar{k}\tilde{H}_1 = Z_i\bar{k}(3-i\chi\bar{v}_0)e^{(1-i\chi\bar{v}_0)\bar{k}\psi}, \quad (24)$$

where $\bar{v}_0=|\vec{\bar{v}}_0|$,

$$\bar{k} = \sqrt{(k_x\beta_x)^2+(k_y\beta_y)^2+(k_z\beta_z)^2}, \quad (25)$$

and $\chi \equiv \vec{k}\cdot\vec{v}_0/\bar{k}\bar{v}_0$. The derivative is with respect to the normalized time ψ. $\tilde{H}_1(\vec{k},t)$ is as defined in Sec. III A. With the

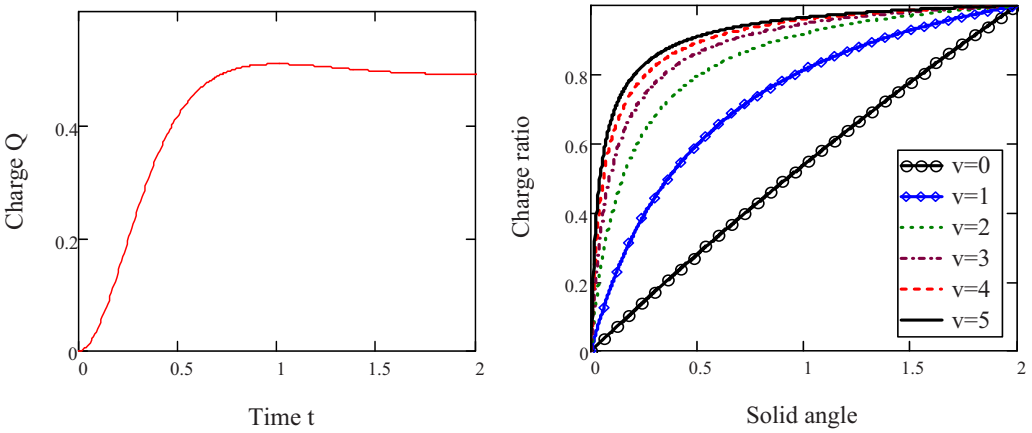

FIG. 5. (Color online) Integrated electron charge induced by a moving ion inside a certain solid angle and radius. (a) Total induced electron charge inside a sphere with radius $\bar{r}_c=2$ as a function of time, and (b) angular charge distribution. The horizontal axis is the solid angle of the backward cone in units of 2π and the vertical axis is $\tilde{Q}(\theta_c)/\tilde{Q}(\pi)$, where the radial cutoff is $\bar{r}_c=5$ and the snapshots are taken at $\psi=2\pi$.

help of initial conditions $\tilde{H}_1(0)=0$, $\tilde{H}_1'(0)=0$, and $\tilde{H}_1''(0)=Z_i$, Eq. (24) can be analytically solved [11] and the electron-density response in the wave-vector domain is

$$\tilde{n}_1(\vec{k},t)=\frac{Z_i}{1+\eta\lambda^2}\left\{1+\tilde{c}_1 e^{-(\lambda+\gamma_0)\psi}-e^{-(\lambda-\gamma_0/2)\psi}\times\left[(1+\tilde{c}_1)\cos(\gamma_1\psi)+\frac{\lambda}{\gamma_1}\left(1-\frac{\gamma_0}{2\lambda}(1+3\tilde{c}_1)\right)\times\sin(\gamma_1\psi)\right]\right\}, \tag{26}$$

where $\lambda(\vec{k})$ is defined in Eq. (13) and $\eta(\vec{k})$, $\gamma_0(\bar{k})$, $\gamma_1(\bar{k})$, and $\tilde{c}_1(\vec{k})$ are functions of the wave vector defined as

$$\gamma_0(\bar{k})\equiv\left(\sqrt{\bar{k}^2+\frac{1}{27}}+\bar{k}\right)^{1/3}-\left(\sqrt{\bar{k}^2+\frac{1}{27}}-\bar{k}\right)^{1/3},$$

$$\gamma_1(\bar{k})\equiv\frac{\sqrt{3}}{2}\left[\left(\sqrt{\bar{k}^2+\frac{1}{27}}+\bar{k}\right)^{1/3}+\left(\sqrt{\bar{k}^2+\frac{1}{27}}-\bar{k}\right)^{1/3}\right],$$

$$\eta(\chi)\equiv 1-\frac{2}{3-i\chi\bar{v}_0},$$

$$\tilde{c}_1(\vec{k})\equiv-\frac{\lambda^2(1-\eta)+\gamma_0^2}{3\gamma_0^2+1}.$$

Equation (26) has a few major differences compared with Eq. (16). First, the frequency of the plasma oscillation now is a function of the wavelength. Second, the Landau damping rate is reduced, especially at long wavelength, since γ_0 is always a positive number and behaves as $\bar{k}^{1/3}$ at large $\bar{k}$, while $\lambda(\vec{k})$ depends linearly on $\bar{k}$. Third, the factor η appears in the factor outside the brackets; it is $\frac{1}{3}$ for $v_0=0$. This factor is important when comparing the results of different velocity distributions. Last, there is a fast-damping term in the brackets, and its damping proceeds far faster than the Landau damping of the plasma oscillation. Fourier inversion of Eq. (26) is too complicated to be analyzed manually. The numerical results are shown in the following section, and compared with those for the Maxwellian plasma and the second-power Lorentzian plasma.

IV. COMPARISON WITH THE MAXWELLIAN PLASMA

The Maxwellian plasma is the most often considered and a more realistic plasma than the Lorentzian plasma. The velocity distribution of the Maxwellian electron plasma is

$$f_0(\vec{v})=\frac{n_0}{(2\pi)^{3/2}\sigma_x\sigma_y\sigma_z}\exp\left(-\frac{(v_x+v_{0x})^2}{2\sigma_x^2}-\frac{(v_y+v_{0y})^2}{2\sigma_y^2}-\frac{(v_z+v_{0z})^2}{2\sigma_z^2}\right), \tag{27}$$

where σ_x, σ_y, and σ_z are the rms spreads of the electron thermal velocities. Unlike a Lorentzian plasma, it defines the average value for any power of the velocities and is naturally reached through collision processes. Unfortunately, the analytic approach for describing the Maxwellian plasma dynamics is usually difficult; the solution of the integral equation (8) must be found numerically. However, since Eq. (8) has no singularity at $t=t_1$, the numerical solution is straightforward. After inserting Eq. (27) and carrying out the integration for the inhomogeneous part, we can write Eq. (8) as

$$\tilde{H}_1(\vec{k},t)=\int_0^{\psi}\tilde{H}_1(\vec{k},\tau)W(\psi-\tau)d\tau+G(\psi), \tag{28}$$

where $\tilde{H}_1(\vec{k},t)\equiv\tilde{n}_1(\vec{k},t)e^{-i\vec{k}\cdot\vec{v}_0 t}$ and $W(\tau)\equiv-\tau e^{-(\bar{k}\tau)^2/2}$. The integration of the inhomogeneous part reads

$$G(\psi)=\frac{Z_i}{\bar{k}^2}\left\{e^{-i\bar{k}\bar{v}_0\chi\psi}\left[1+i\sqrt{\frac{\pi}{2}}\bar{v}_0\chi w\left(\frac{\bar{v}_0\chi}{\sqrt{2}}\right)\right]-e^{-(\bar{k}\psi)^2/2}\left[1+i\sqrt{\frac{\pi}{2}}\bar{v}_0\chi w\left(i\sqrt{2}\bar{k}\psi+\frac{\bar{v}_0\chi}{\sqrt{2}}\right)\right]\right\},$$

where $w(z)\equiv e^{-z^2}\mathrm{Erfc}(-iz)$ is the Faddeeva function. Equation (28) is a Volterra equation of the second type that can be solved simply by iteration. Figure 6 shows the responses of the second-power Lorentzian, third-power Lorentzian, and Maxwellian plasmas to an ion moving with velocity $\bar{v}_0=0$, 0.5, 1, and 3. Clearly, they exactly overlap with each other for $\vec{v}_0=\vec{0}$. (We will show later that in order to have the same Debye radius at $\vec{v}_0=\vec{0}$, for the second-power Lorentzian plasma $\sigma_i=\beta_i$ and for the third-power Lorentzian plasma $\sigma_i=\beta_i/\sqrt{3}$.) Since normalized variables are used in the calculations, Fig. 4 also describes the anisotropic plasmas. As Eq. (20) shows, the analytic black curve in Fig. 6(a) represents an exponential decay, which suggests that the responses of the other two plasmas to a rest ion also exponentially decay, regardless of whether or not the plasma is isotropic. Provided that the velocity distribution has elliptical symmetry, the response of the electron plasma to a rest ion always exponentially decays with the distance. This is verified in the following. By making a Laplace transformation of Eq. (4), the electron density response in $(\vec{k},p)$ space can be written as

$$\tilde{n}_1(\vec{k},p)=-i\frac{Z_i}{p}\frac{\frac{\omega_p^2}{k^2}\int\frac{\vec{k}\cdot\frac{\partial}{\partial\vec{v}}f_0(\vec{v})}{p+i\vec{k}\cdot\vec{v}}d^3v}{1-i\frac{\omega_p^2}{k^2}\int\frac{\vec{k}\cdot\frac{\partial}{\partial\vec{v}}f_0(\vec{v})}{p+i\vec{k}\cdot\vec{v}}d^3v}, \tag{29}$$

where

$$\tilde{n}_1(\vec{k},p)=\int_0^{\infty}\tilde{n}_1(\vec{k},t)e^{-pt}dt.$$

The electron response in the time domain then is obtained by inversely transforming Eq. (29) according to the following formula:

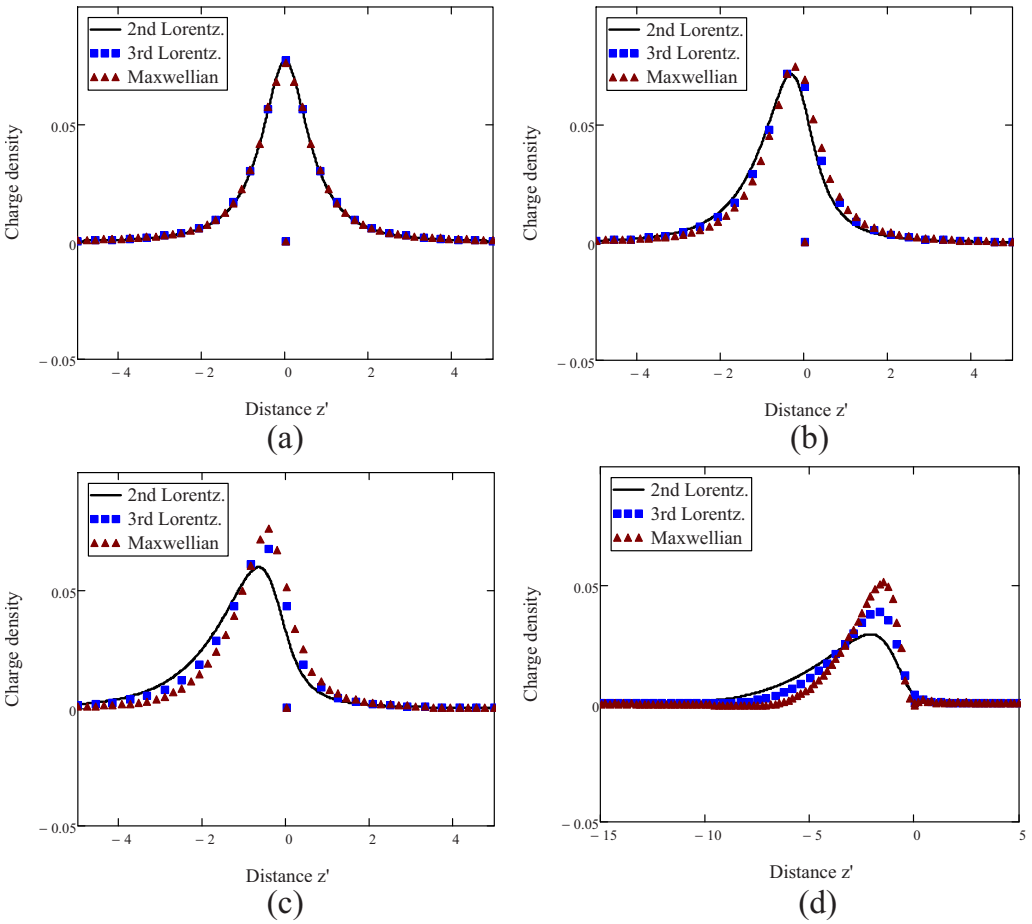

FIG. 6. (Color online) Responses of three different electron plasmas to an ion moving with various velocities. (a) is for a rest ion, (b) is for $\bar{v}_0=0.5$, (c) is for $\bar{v}_0=1$, and (d) is for $\bar{v}_0=3$. The horizontal axis is the longitudinal distance from the ion in units of the longitudinal Debye radius and the vertical axis is the induced electric charge per Debye volume. The snapshot is taken at $\psi=\pi$.

$$\tilde{n}_1(\vec{k},t)=\frac{1}{2\pi i}\int_{-i\infty+\sigma}^{i\infty+\sigma}\tilde{n}_1(\vec{k},p)e^{pt}dp. \tag{30}$$

The integral in Eq. (30) is calculated by summing up all the residues at the poles of $\tilde{n}_1(\vec{k},p)$. All poles obtained from solving the dispersion relation

$$1-i\frac{\omega_p^2}{k^2}\int\frac{\vec{k}\cdot(\partial/\partial\vec{v})f_0(\vec{v})}{p+i\vec{k}\cdot\vec{v}}d^3v=0 \tag{31}$$

go to zero with $t\to\infty$, and only the pole at $p=0$ survives at equilibrium. Consequently, the electron response at equilibrium can be obtained by calculating just the residue at $p=0$. Assuming that the velocity distribution of the electron plasma has elliptical distribution, i.e.,

$$f_0(\vec{v})=f_0(\bar{v}),$$

where $\bar{v}=\sqrt{v_x^2/\beta_x^2+v_y^2/\beta_y^2+v_z^2/\beta_z^2}$, the integral in Eq. (29) for $p=0$ can be simplified to

$$\frac{\omega_p^2}{k^2}\int\frac{\vec{k}\cdot(\partial/\partial\vec{v})f_0(\vec{v})}{p+i\vec{k}\cdot\vec{v}}d^3v=i\frac{4\pi\beta_x\beta_y\beta_z}{\bar{k}^2}\int_0^\infty f_0(\bar{v})d\bar{v}. \tag{32}$$

Inserting Eq. (32) into Eq. (29) gives

$$\tilde{n}_1(\vec{k},t\to\infty)=\frac{Z_i}{1+\eta_0\bar{k}^2}, \tag{33}$$

where

$$\eta_0\equiv\frac{1}{4\pi\beta_x\beta_y\beta_z\int_0^\infty f_0(\bar{v})d\bar{v}}. \tag{34}$$

The inverse Fourier transformation of Eq. (33) generates

$$\tilde{n}_1(\vec{x},t\to\infty)=\frac{Z_i}{4\pi a_x a_y a_z}\frac{e^{-\bar{r}}}{\bar{r}}, \tag{35}$$

where $a_i\equiv\sqrt{\eta_0}\beta_i/\omega_p$ and $\bar{r}=\sqrt{x^2/a_x^2+y^2/a_y^2+z^2/a_z^2}$. By calculating η_0 for all three velocity distributions and comparing the results with Eqs. (16) and (26), it is verified that the formula of Eq. (33) is consistent with the previous calculations. Figure 6 also suggests that, for $v_0\leqslant\sigma_e$, both the second- and third-power Lorentzian plasmas behave simi-

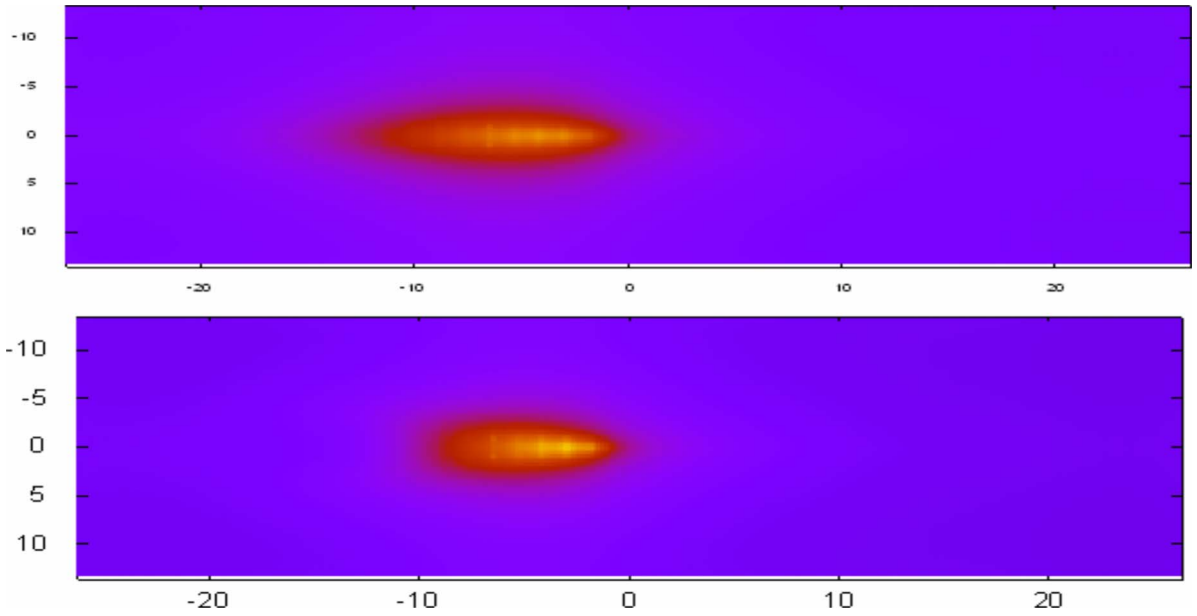

FIG. 7. (Color online) Responses of the electron plasmas to a fast ion. The horizontal axis is the longitudinal distance in units of longitudinal Debye radius and the vertical axis is the transverse distance in units of transverse Debye radius. The top graph is for the second-power Lorentzian plasma and the bottom one is for the Maxwellian plasma. The ion is moving with velocity $v_0=5$ and the snapshot is taken at $\psi=\pi$.

larly to the Maxwellian plasma, but the third-power Lorentzian plasma apparently is better than the second-power one. When v_0 is a few σ_e, the response of the Maxwellian plasma is more localized than that of Lorentzian plasmas as seen in Fig. 7, comparing a snapshot of the Maxwellian with that of the second-power Lorentzian plasma; this comparison is also valid for the third-power Lorentzian plasma.

V. COMPARISON WITH THE ASYMPTOTIC RESULTS

Although the response of the Maxwellian plasma to an ion is difficult to obtain analytically, asymptotic formulas were derived in both the space and the wave-vector domains. Landau in the 1940s [12] found that the dependence of the plasma frequency and Landau damping rate on the wavelength are

$$\omega = \omega_p\left(1 + \frac{3}{2}k^2 r_D^2\right),$$

$$\gamma = \omega_p \sqrt{\frac{\pi}{8}} \frac{1}{(kr_D)^3} \exp\left[-\frac{1}{2(kr_D)^2} - \frac{3}{2}\right]$$

for the isotropic Maxwellian plasma at the limit $kr_D \ll 1$. Figures 8(a) and 8(b) show the plasma frequency and Landau damping rates for all three distributions at the long-wavelength limit. The third-power Lorentzian plasma clearly is much closer to the Maxwellian plasma than is the second-power one at this limit. At the short-wavelength limit, $kr_D \gg 1$, the plasma frequency and Landau damping rate are given by

$$\omega = \omega_p \frac{\pi k r_D}{\xi(\vec{k})},$$

$$\gamma = \omega_p k r_D \xi(\vec{k}),$$

where $\xi(\vec{k})$ is implicitly determined by the following equation:

$$\xi e^{\xi^2/2} = \frac{1}{\sqrt{2}}(kr_D)^2.$$

Since $\xi(\vec{k})$ is a slowly varying function, both the Landau damping rate and the plasma frequency grow linearly with kr_D. As shown in Figs. 8(c) and 8(d), although the behaviors of the Lorentzian plasmas are quite different from that of the Maxwellian plasma in the short-wavelength limit, the third-power Lorentzian distribution still is closer to it than is the second-power Lorentzian distribution.

Several authors have calculated numerical solutions of the stationary electrostatic potential for the Maxwellian plasma in the space domain [6–8]. To compare our results with these previous numerical solutions, the electric potential must be calculated. By combining Eqs. (5) and (17), the time derivative of the electric potential in the $\vec{k}$ domain is

$$\dot{\Phi}(\vec{k},t) = -\frac{Z_i e \omega_p}{\epsilon_0 k^2} \sin(\omega_p t) e^{\lambda(\vec{k})t}. \tag{36}$$

By Fourier transforming Eq. (36) and taking into account the initial condition $\Phi(\vec{x},0)=Z_i e/4\pi\epsilon_0|\vec{x}|$, the electric potential induced by a moving ion in the second-power Lorentzian plasma is obtained as

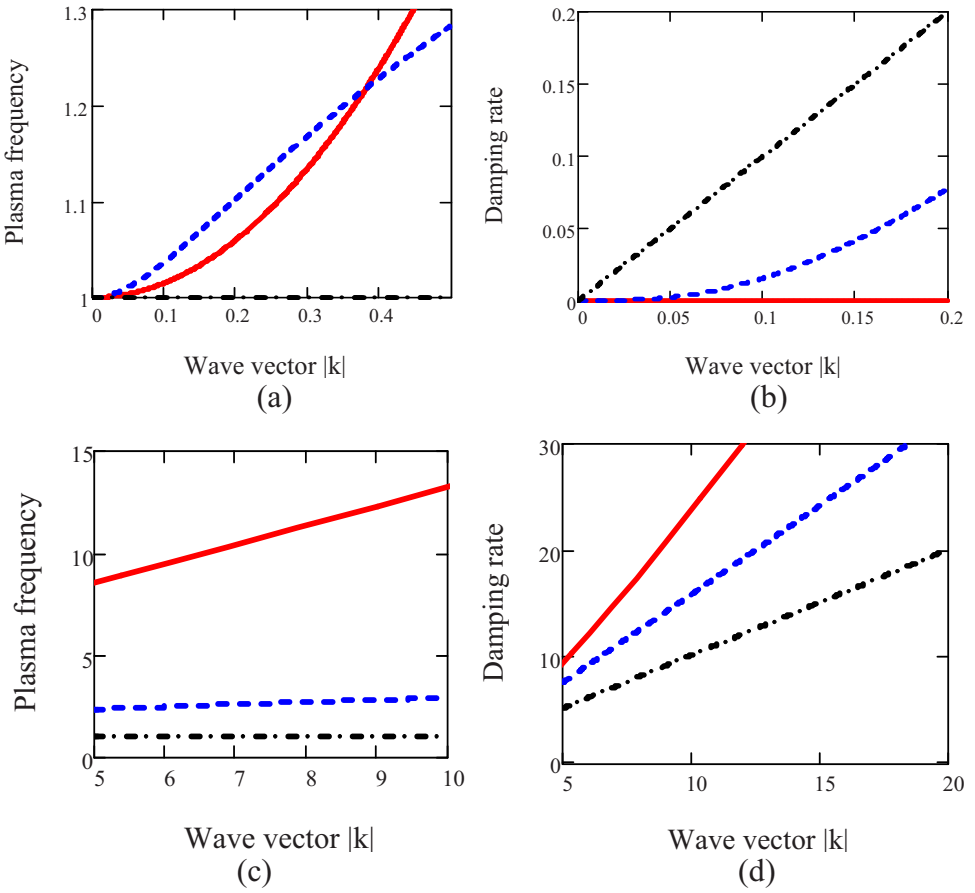

FIG. 8. (Color online) Plasma frequency and Landau damping rate at the limits of long and short wavelengths. The horizontal axis is kr_D. (a) and (b) show the plasma frequency and Landau damping rate in units of ω_p at $kr_D \ll 1$ while (c) and (d) show the other limit $kr_D \gg 1$. The solid (red) line is for the approximate formula for the Maxwellian distribution derived in [12], the dot-dashed (black) line and the dashed (blue) line are for the analytic formulas derived for the second- and third-power Lorentzian distributions, respectively.

$$\Phi(\vec{x},t) = \frac{Z_i e}{4\pi\epsilon_0}\left[\frac{1}{|\vec{x}|} - \frac{2\omega_p}{\pi}\int_0^t \frac{\sin(\omega_p\tau)}{|\vec{x}+\vec{v}_0\tau|} \times \arctan\left(\frac{|\vec{x}+\vec{v}_0\tau|}{\beta\tau}\right)d\tau\right] \tag{37}$$

for $\beta_{x,y,z}=\beta$. Equation (5) also can be used to calculate the electric potential for the Maxwellian plasma by the fast Fourier transform method (FFT) since $\tilde{n}_1(\vec{k},t)$ was already numerically solved. Figure 9 presents the results for the induced electric potential at $\psi \gg 2\pi$. Figure 9(a) shows the analytic result expressed in Eq. (37) for the second-power Lorentzian plasma; the snapshot is taken at $\psi=60\pi$. Compared with the numerical results for the Maxwellian plasma, the results for the Lorentzian plasma agree very well for $v_i \leqslant \sqrt{2}\beta_e$ but the curve flattened more at higher velocities. Figure 9(b) shows the FFT results for the Maxwellian plasma at $\psi \gg 2\pi$, which agree very well with the steady-state results (Fig. 7 of Ref. [6], Fig. 4 of Ref. [8], and Fig. 9 of Ref. [7]). Since the Landau damping is slow for relatively long wavelengths, some small differences at the tail still may exist. As the longitudinal range of the FFT calculation is limited by the computer's memory and solution of the dynamical equation (28) for a very long time range is also time consuming, Fig. 9(b) shows results only for a relatively short time range, and $v_i \leqslant 2\sqrt{2}\sigma_e$.

The steady-state effective potential of a rest ion in an anisotropic plasma was calculated by Montgomery *et al.* in the 1960s and an inverse-third-power law at large distance was found [3]. Since we have obtained the steady-state electron density response for a rest ion in Eq. (35), the electric potential can be calculated by using the multipole moments expansion. From Eq. (35), the total induced charge is

$$-e\int\int\int \tilde{n}_1(\vec{x},t\to\infty)dV = -Z_i e,$$

which exactly cancels the charge of the ion. The dipole moment also vanishes as $\tilde{n}_1(\vec{x},t\to\infty)$ is an even function of x, y, and z. Thus the dominant term at the large distance is from the quadrupole moment,

$$\Phi(\vec{x}) = \frac{1}{4\pi\epsilon_0}\frac{1}{2}\sum_{i,j} Q_{ij}\frac{x_i x_j}{r^5}, \tag{38}$$

where

$$Q_{ij} = -e\int\int\int (3x_i x_j - r^2\delta_{ij})\tilde{n}_1(\vec{x},t\to\infty)dV. \tag{39}$$

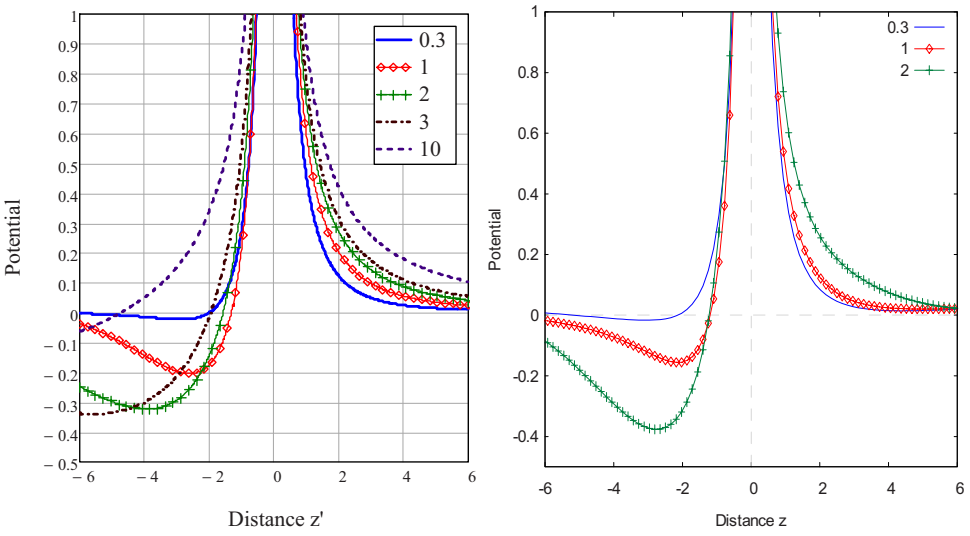

FIG. 9. (Color online) Electric potential along the z axis for various ion speeds. The horizontal axis is the longitudinal distance from the moving ion and the vertical axis is the electrical potential in units of $Z_i e/r_D$. (a) The analytic results for the second-power Lorentzian plasma at $\psi=60\pi$, and, (b) the numerical results for the Maxwellian plasma. The curves $v_0/\sqrt{2}\sigma_e=1$ (red) and 2 (green) curve were taken at $\psi=7\pi$ and the $v_0/\sqrt{2}\sigma_e=0.3$ curve (blue) at $\psi=15\pi$.

From Eqs. (35), (38), and (39), the electric potential due to the quadrupole moment is

$$\Phi(\vec{x}) = \frac{Z_i e}{4\pi\epsilon_0 r^5}[(a_y^2 + a_z^2 - 2a_x^2)x^2 + (a_x^2 + a_z^2 - 2a_y^2)y^2 + (a_x^2 + a_y^2 - 2a_z^2)z^2]. \quad (40)$$

If $\beta_x=\beta_y=\beta_\perp$ and $\beta_z\equiv\beta_\parallel$, Eq. (40) reduces to

$$\Phi(\vec{x}) = \frac{Z_i e\beta_\perp^2}{2\pi\epsilon_0 r^3\omega_p^2}\left(1-\frac{\beta_\parallel^2}{\beta_\perp^2}\right)\left(1-\frac{3}{2}\frac{x^2+y^2}{r^2}\right), \quad (41)$$

which reproduces Eq. (18) in Ref. [3].

VI. SUMMARY

The dynamic model described in Secs. II and III depends on the choice of the velocity distribution. This dependence seems to be weak while the ion is moving with velocity $v_i \leqslant \sigma_e$. Consequently, the analytic formula obtained for the Lorentzian distribution can describe the process with good accuracy. For fast ions, the effects due to the thermal distribution strengthen, but for ion velocities up to a few σ_e, the formula obtained for the third-power Lorentzian distribution still can serve as a qualitative estimation. The numerical solution for the Maxwellian distribution is straightforward under our model and might be much faster than particle in cell simulations. As discussed in Sec. IV, the electron density response for a rest ion in an anisotropic plasma seemingly decays exponentially, which generates a quadrupole-type electric potential at large distance.

ACKNOWLEDGMENTS

We would like to thank Ilan Ben-zvi and V. N.Litvinenko for suggesting and helping with this subject. We would also like to thank D. Montgomery for pointing out our mistakes in earlier versions of the manuscript.

[1] Ya. S. Derbenev, in *Proceedings of Seventh All-Union Conference on Charged Particle Accelerators* (Dubna, USSR, 1980), p. 269.
[2] V. N. Litvinenko and Ya. S. Derbenev, in *Proceedings of 29th International Free Electron Laser Conference*, edited by B. Goldenberf, V. Eliseev, A. Zhirkova, and P. Budz (Budker INP, Novosibirsk, Russia, 2007), p. 268; http://accelconf.web.cern.ch/accelconf/f07/
[3] D. Montgomery, G. Joyce, and R. Sugihara, Phys. Fluids **10**, 681 (1968).
[4] G. Cooper, Phys. Fluids **12**, 2707 (1970).
[5] C. R. James and F. Vermeulen, Can. J. Phys. **48**, 349 (1970).
[6] C.-L. Wang, G. Joyce, and D. R. Nicholson, J. Plasma Phys. **25**, 225 (1981).
[7] E. W. Laing, A. Lamont, and P. J. Fielding, J. Plasma Phys. **5**, 441 (1971).
[8] P. Chenevier, J. M. Dolique, and H. Peres, J. Plasma Phys. **10**, 185 (1973).
[9] A. J. Turski, Ann. Phys. (N.Y.) **35**, 240 (1965).
[10] A. J. Turski, Ann. Phys. **22**, 180 (1969).
[11] T. Harriet, URL: http://locke.citizendium.org:8080/wiki/Solving_cubic_equations
[12] L. Landau, J. Phys. (USSR) **10**, 25 (1946).